PNAS RESEARCH ARTICLE | APPLIED PHYSICAL SCIENCES

Rubber-glass nanocomposites fabricated using mixed emulsions

Zheqi Chen[a,b,1], Guogao Zhang[a,1], Yingwu Luo[b], and Zhigang Suo[a,2]

Contributed by Zhigang Suo; received December 22, 2023; accepted February 22, 2024; reviewed by Michael D. Dickey and Kenneth Shull

Many composites consist of matrices of elastomers and nanoparticles of stiff materials. Such composites often have superior properties and are widely used. Embedding elastomers with nanoparticles commonly necessitates intense shear, using machines like extruders and roll millers, which cut polymer chains and degrade properties. Here, we prepare a rubber-glass nanocomposite by using two aqueous emulsions. Each emulsion is separately prepared with a single species of polymer chains. Each polymer chain is copolymerized with a small amount of silane coupling agent. Upon mixing the two emulsions, as water evaporates, the glassy particles retain the shape, and the rubbery particles change shape to form a continuous matrix. Subsequently, the silane coupling agent condensates, which cross-links the rubbery chains and interlinks the rubbery chains to the glassy particles. The cross-links and interlinks stabilize the nanostructure and lead to superior properties. The nanocomposite simultaneously achieves high modulus (~30 MPa), high toughness (~100 kJ m^{-2}), and high fatigue threshold (~1,000 J m^{-2}). The method of mixed emulsion is environmentally friendly and compatible with various open-air manufacturing processes, such as coat, cast, spray, print, and brush. Additionally, the silane coupling agent can interlink the nanocomposite to other materials. The method of mixed emulsion can be used to fabricate objects of complex shapes, fine features, and prescribed spatial variations of compositions.

polymers | fracture | fatigue | nanocomposites | emulsions

Significance

Polymer nanocomposites can be made by blending polymers, but the intense shear cuts polymer chains and degrades properties. Nanocomposites can also be made by mixing monomers and then polymerizing, but the monomers are often volatile and toxic, preventing the nanocomposites from being fabricated in open air. We fabricate rubber-glass nanocomposites by mixing two aqueous emulsions. Each emulsion is prepared separately with a single species of polymer chains, and each polymer chain is copolymerized with a silane coupling agent. As water evaporates, the silane coupling agent condensates, linking the polymer chains. The nanocomposite simultaneously achieves high modulus, high toughness, and high fatigue threshold. The method is applicable to various polymers and enables environmentally friendly manufacturing processes in open air.

Superior properties are often achieved by nanocomposites in which matrices of elastomers embed nanoparticles of stiff materials (1–4). For example, elastomers embedding carbon nanoparticles achieve high modulus, toughness, and wear resistance—properties that are essential for tires, belts, coatings, etc (5). Embedding elastomers with nanoparticles commonly necessitates intense shear, using machines like extruders and roll millers. Such high-intensity processes cut polymer chains and degrade properties (6, 7). This challenge is met by mixing nanoparticles with liquid monomers, followed by polymerizing the monomers (8). However, the monomers are often volatile and toxic, preventing the nanocomposites from being fabricated in open air.

Here, we report a method to fabricate rubber-glass nanocomposites of superior properties (Fig. 1). The method requires, during mixing, neither high-intensity processes nor monomers. Rather, we fabricate the nanocomposites by mixing two aqueous emulsions. One emulsion contains a rubbery polymer poly(ethyl acrylate) (PEA), and the other emulsion contains a glassy polymer poly(methyl methacrylate) (PMMA). Each emulsion is separately prepared with a single species of uncross-linked polymer chains, each polymer chain is copolymerized with a small amount of silane coupling agent, and each emulsion particle is covered with a surfactant (Fig. 1*A*). At room temperature, the silane coupling agent does not condensate, and the surfactant prevents the emulsion particles from coagulation. The viscosities of the emulsions are similar to that of water so that the two emulsions can be easily mixed (Fig. 1*B*). As water evaporates from the mixed emulsion, the glassy particles retain shape, but the rubbery particles change shape to form a continuous matrix (Fig. 1*C*). Subsequently, the silane coupling agents condensate into siloxane linkages, which cross-link the rubbery polymer chains, and interlink the rubbery chains to the glassy particles.

For the rubber-glass nanocomposite, the cross-links and interlinks stabilize the nanostructure and lead to superior properties. For example, the nanocomposite of 40 vol.% of PMMA simultaneously achieves a modulus of 30 MPa, toughness of 91 kJ m^{-2}, and fatigue threshold of 1,100 J m^{-2}. This combination of excellent properties is rarely achieved among polymeric materials, as shown on the plane of toughness and modulus, as well as on the plane of toughness and fatigue threshold (Fig. 2).

The mixed emulsions enable environmentally friendly fabrication of nanocomposites. The method divides the labor between the emulsion maker and the emulsion user. The maker can produce emulsions on a large scale in a facility that controls volatile compounds, such as monomers and organic solvents. The emulsions, once produced, contain no volatile

Author contributions: Z.C., G.Z., and Z.S. designed research; Z.C. performed research; Z.C., G.Z., Y.L., and Z.S. analyzed data; and Z.C., G.Z., and Z.S. wrote the paper.

Reviewers: M.D.D., North Carolina State University; and K.S., Northwestern University.

The authors declare no competing interest.

[1]Z.C. and G.Z. contributed equally to this work.

[2]To whom correspondence may be addressed. Email: suo@seas.harvard.edu.

This article contains supporting information online at https://www.pnas.org/lookup/suppl/doi:10.1073/pnas.2322684121/-/DCSupplemental.

Published April 8, 2024.

compounds and are stable for long-distance distribution and long-time storage. The user is safe to mix and dry the emulsions in open air. Consequently, the method of mixed emulsion is compatible with various open-air manufacturing processes, such as coat, cast, spray, print, and brush. The method of mixed emulsion can be used to fabricate objects of complex shapes, fine features, and prescribed spatial variations of compositions. Additionally, the silane coupling agents can interlink the nanocomposites to other materials to form strong adhesion.

Results and Discussion

We prepare two emulsions separately by radical polymerization (*SI Appendix*, Fig. S1). One emulsion contains particles of a rubbery polymer, poly(ethyl acrylate) (PEA). The other emulsion contains particles of a glassy polymer, poly(methyl methacrylate) (PMMA). During the synthesis of each emulsion, the monomer is copolymerized with a small amount of a silane coupling agent, 3-(trimethoxysilyl)propyl methacrylate (TMSPMA). Dynamic light scattering profiles show that the diameters of PEA and PMMA emulsion particles are ~ 110 nm and ~ 90 nm, respectively (*SI Appendix*, Fig. S2). In the emulsion, the methylsilyl groups $-Si(OCH_3)_3$ in the TMSPMA hydrolyze to form silanol groups $-Si(OH)_3$. The exterior of each emulsion particle is covered with a surfactant, sodium dodecyl sulfate. Each emulsion is stable for at least 8 mo, during which neither the silanol groups condensate, nor the emulsion particles coagulate.

Each emulsion contains ~27 wt% of polymer. The two emulsions flow readily and can be mixed by mild hand shake (Fig. 3*A*). We pour the mixed emulsion into a petri dish. As the water evaporates at 45 °C, the silanol groups condensate to form siloxane linkages, which cross-link the PEA chains and interlink PEA chains to PMMA particles. After almost all the water evaporates at 45 °C, the sample is kept at 65 °C for 1 d to remove the residual water and accelerate the condensation of the silanol groups. The small amount of surfactant is likely to precipitate out upon drying due to its incompatibility to the dry polymers (12). Eventually, a film of the rubber-glass nanocomposite is obtained (Fig. 3*B*). The PEA-PMMA nanocomposite of a high PMMA volume fraction is semitransparent (*SI Appendix*, Fig. S3). The scattering is ascribed to the different refractive indices of PEA (1.4685) and PMMA (1.4893). The situation is similar to that of a PDMS-PMMA nanocomposite (13).

We prepare the nanocomposites with various ratios of the two emulsions and observe the nanocomposites using an atomic force microscope (AFM) (Fig. 3*C*). We denote the PEA-PMMA nanocomposite of a PMMA volume fraction ϕ by PEA-PMMAϕ. After water is removed, the glassy PMMA particles retain shape, and the rubbery PEA particles flow into a space-filling matrix. As ϕ increases, PMMA particles cluster. Between two PMMA particles in proximity, a thin layer of PEA is observed. This observation is understood as follows. Two glassy PMMA particles are rigid and only form point-like contact, leaving void space between the particles. The high curvature of the void space and the surface energy between the polymer and air drive the rubbery PEA to flow and fill the void space. In the absence of cross-links and interlinks, the PEA chains and PMMA particles are mobile so that the PMMA particles will migrate, and the nanocomposite will separate into PMMA-rich regions and PMMA-poor regions. The two regions will coarsen in time (*SI Appendix*, Fig. S4) (14). After cross-links and interlinks form, coarsening is arrested and the nanostructure is stable (*SI Appendix*, Fig. S5). No high-intensity process is needed to disperse emulsion particles of dissimilar polymers.

The PMMA particles are hard spheres randomly embedded in the PEA matrix. In such a composite, the critical volume fraction for particles to percolate is ~18%, at which a cluster spans the whole material (15, 16). The maximum volume fraction of the particles is ~60% (15, 16). These theoretical values are consistent with our experimental observations. When the volume fraction of PMMA exceeds 60%, the fraction of PEA is too low to form a

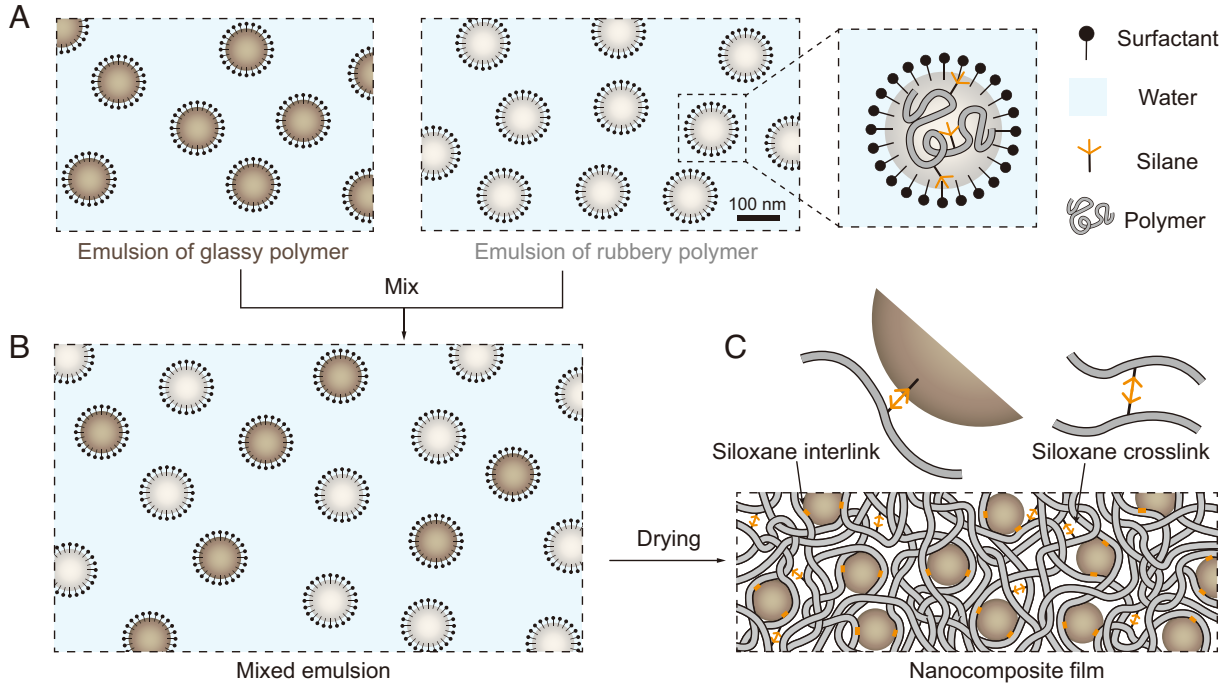

Fig. 1. A rubber-glass nanocomposite fabricated by mixing an emulsion of rubbery polymer and an emulsion of glassy polymer. (*A*) Each aqueous emulsion is prepared separately, containing a single species of polymer chains copolymerized with a silane coupling agent. The exterior of every emulsion particle is covered with a surfactant. (*B*) Mix the two emulsions. (*C*) Upon drying, the glassy particles retain shape, but the rubbery particles change shape to form a continuous matrix. The silane coupling agents condensate into siloxane linkages, which cross-link the rubbery chains and interlink the rubbery chains to glassy particles.

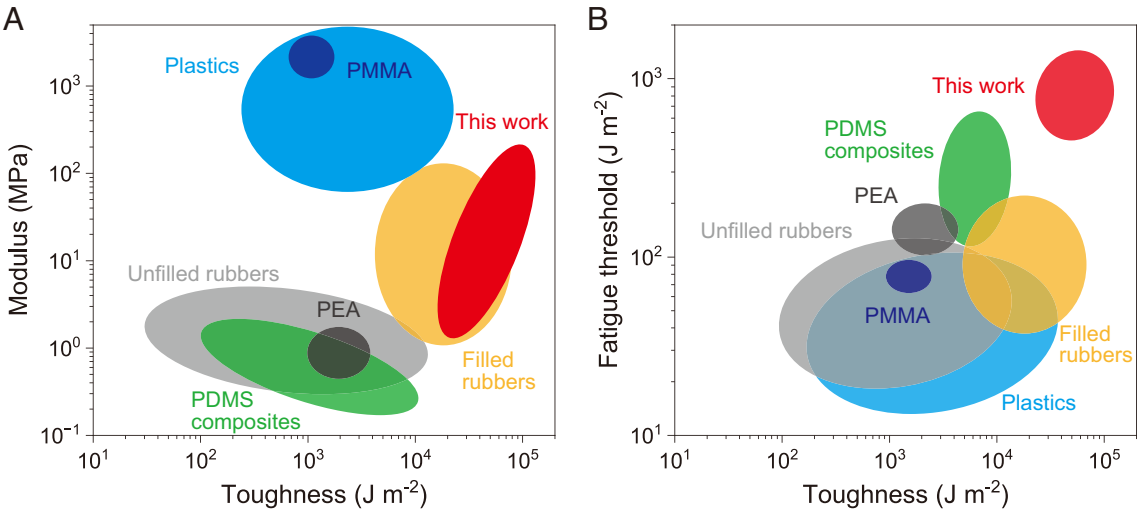

Fig. 2. Rubber-glass nanocomposites prepared in this work are compared with existing polymeric materials on (*A*) the plane of modulus and toughness and (*B*) the plane of fatigue threshold and toughness. Data are collected from published papers (9, 10). PDMS composites refer to composites of hard PDMS and soft PDMS (9, 11).

space-filling matrix so that the dry film is porous and forms cracks (*SI Appendix*, Fig. S6).

We measure stress–stretch curves of the nanocomposites (Fig. 4*A*). Depending on the volume fraction of PMMA, the modulus ranges over two orders of magnitude (Fig. 4*B*). The modulus exhibits a significant increase due to the percolation of the PMMA particles at a high volume fraction. The enhancement in modulus is beyond the Guth–Gold solution for a composite of rigid spherical particles in a linear elastic matrix (17), and can be described by a composite model proposed by Kotula and Migler (*SI Appendix*, Fig. S7) (18, 19).

All the nanocomposites show higher tensile strength and higher work of fracture than those of pure PEA (Fig. 4*C*). Notably, when $\phi \geq 20\%$, during uniaxial tensile test, the sample fractures by cracks running parallel to the stretching direction (*SI Appendix*, Fig. S8). This observation is likely attributed to the percolation of PMMA particles, which generates a fiber-like structure in the nanocomposite.

When PMMA particles highly percolate ($\phi = 40\%$), the nanocomposite exhibits pronounced hysteresis during loading and unloading, but the permanent deformation after unloading is small (Fig. 4 *D* and *E*). After the first loading to a stretch of 3 and subsequent unloading, we hold samples at room temperature for various times and then reload the sample (Fig. 4*D*). The strain at which the stress changes from negative to zero during the reloading is recorded as the residual strain. As the holding time increases, the residual strain reduces. After 8 h of holding at room temperature, the residual strain is 2%, and the sample can recover 79% of its original tensile stress. In a separate experiment, after loading and unloading a sample, we hold the sample at 65 °C for 12 h. The sample fully recovers and has a nearly identical stress–stretch curve to that of the pristine sample. We then fix the holding time of 2 min at room temperature and record the residual strains after the sample is loaded to different strains (Fig. 4*E*). In all the cases, the residual strains remain below 7% of the applied peak strain.

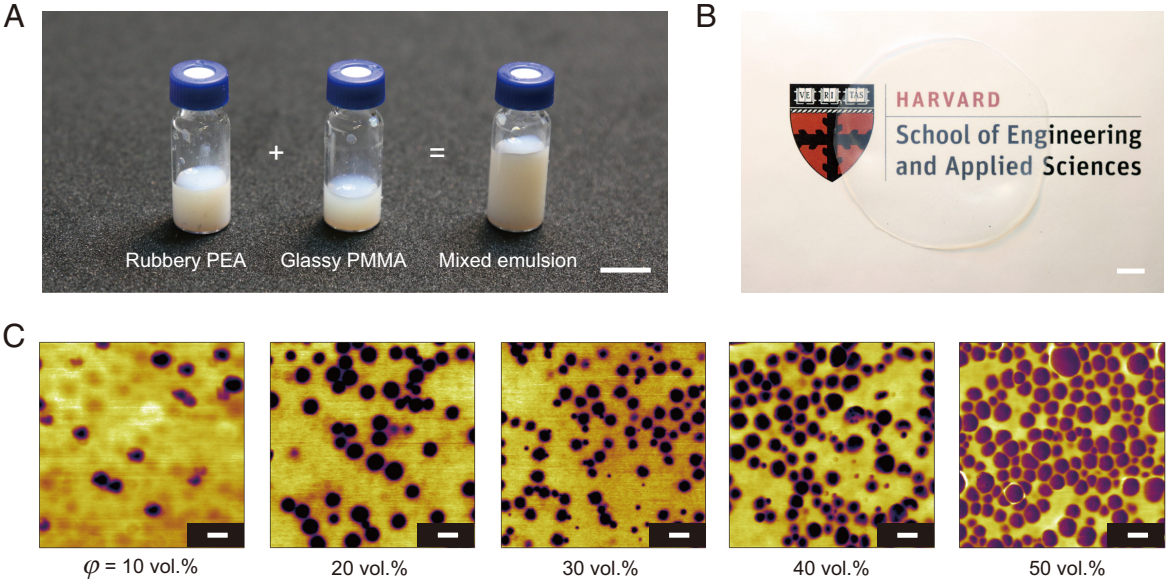

Fig. 3. PEA-PMMA nanocomposites fabricated using a mixed emulsion. (*A*) Photos of PEA emulsion, PMMA emulsion, and their mixture. The scale bar represents 10 mm. (*B*) Photos of the nanocomposite PEA-$PMMA_{40}$ The scale bar represents 10 mm. (*C*) Atomic force microscopy images of the rubber-glass nanocomposites of various compositions. The dark-color regions represent the PMMA phase, and the light-color regions represent the PEA phase. The scale bars represent 100 nm.

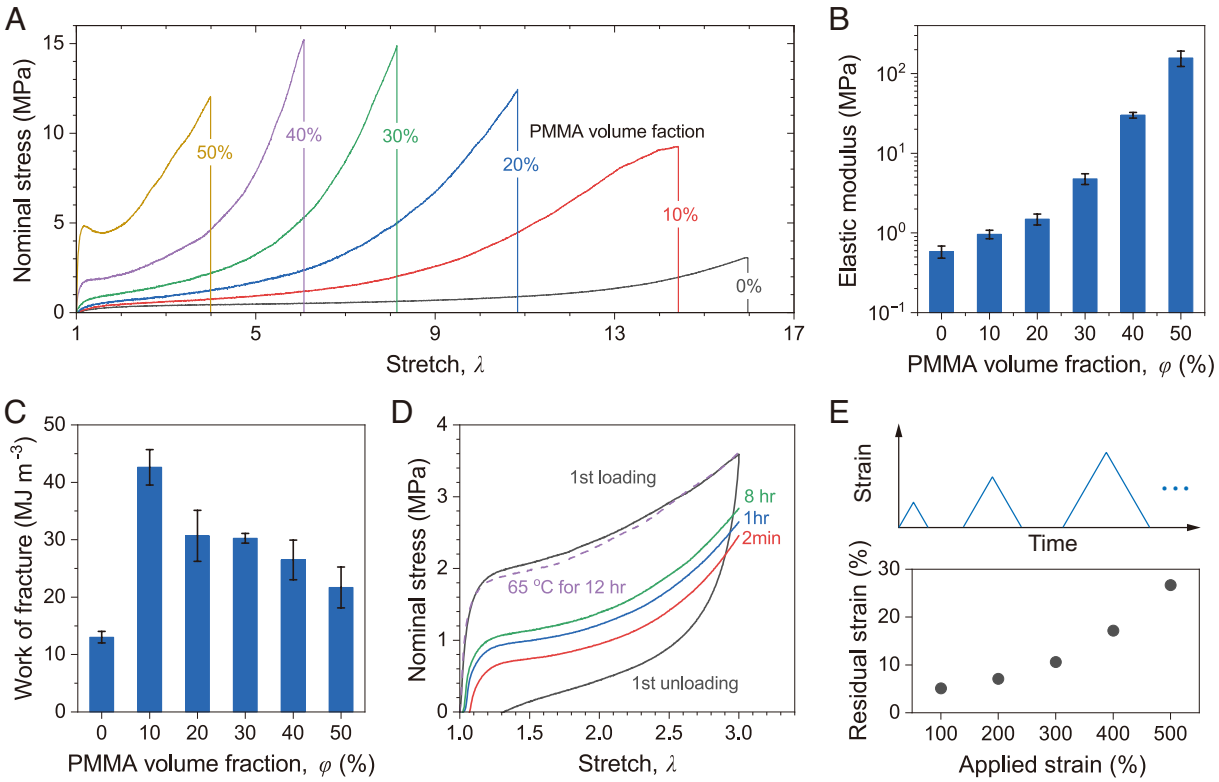

Fig. 4. Stress–stretch curves of rubber-glass nanocomposites of various compositions. (*A*) Stress–stretch curves under monotonic tension. (*B*) Elastic modulus. Error bars indicate the SEM; $n = 3$ for each group. (*C*) Work of fracture. Error bars indicate SEM; $n = 3$ for each group. (*D*) Loading and unloading curves of PEA-$PMMA_{40}$. Solid curves are reloading curves after being stored at room temperature for different periods. The dashed curve is the reloading curve after being stored at 65 °C for 12 h. (*E*) The residual strains after being stretched to different strains. The stretch rate is 0.05 s^{-1}.

These observations are consistent with the following interpretations. The stress is low enough so that the PMMA particles deform negligibly. The full recovery of the stress–stretch curve after holding the sample at an elevated temperature indicates that the sample is not damaged during the first loading and unloading. The hysteresis is due to viscoelasticity. Recall that the pure PEA has relatively small hysteresis (20). The large hysteresis observed here for the nanocomposite is likely due to the reversible detachment and adsorption of PEA chains at the interface of PEA and PMMA under large deformation (1). The interlinks between the PEA chains and PMMA particles are strong but sparse. The large deformation does not break the interlinks but may cause the PEA chains between the interlinks to detach from the PMMA particles and reattach. Under small deformation, the loss tangent (tanδ) of the nanocomposite is 0.27, which is comparable to that of pure PEA (0.16).

The percolated structure of PMMA particles makes the nanocomposite resist crack growth. For PEA-$PMMA_{40}$, the nanocomposite is notch-insensitive under monotonic load. We stretch the sample with a precrack and watch the crack run during a pure shear test (Fig. 5*A* and Movie S1). Even with the precrack, the sample can be pulled to a stretch exceeding 5. During the stretch, the crack blunts and bifurcates, with the bifurcated cracks running in the direction perpendicular to that of the precrack (Fig. 5*B*). The bifurcation deconcentrates stress at the crack tip and results in high toughness (Fig. 5*C*). The crack bifurcation is typically observed in a fiber-reinforced composite (9, 11) or a material capable of stress-induced crystallization (21). The nanocomposite here does not have fibers, nor does it undergo stress-induced crystallization. The crack bifurcation here is likely due to the PMMA nanoparticles percolating into fiber-like structures, which align in front of the crack when the material is stretched. For a nanocomposite with a high volume fraction of PMMA, the size of the inelastic zone may be too large to fulfill the small-scale inelasticity conditions. Consequently, the toughness of the nanocomposite, which ought to be measured under the small-scale inelasticity conditions, might be even larger than the value reported here. This point is not studied in the current paper. In Fig. 4*A*, the tensile stress–stretch test was conducted by using a sample of the dog-bone shape. In Fig. 5*A*, the toughness test was conducted by pure shear, using a sample whose width (60 mm) is far larger than its height (10 mm). The uniaxial tensile and pure shear are different in the boundary conditions, which leads to the difference in value of stress.

Toughness divided by work of fracture defines a quantity with a dimension of length, called the fractocohesive length (22, 23). The fractocohesive length measures the flaw sensitivity of a material. When flaws are smaller than the fractocohesive length, the extreme mechanical properties, such as strength and ultimate stretch, are insensitive to the presence of flaws. The nanocomposites are insensitive to millimeter-scale cracks (Fig. 5*D*). For example, the fractocohesive length of PEA-$PMMA_{40}$ is ~4 mm.

We next characterize the precracked nanocomposites under cyclic load. The crack growth per cycle, dc/dn, is measured at various amplitudes of energy release rate (Fig. 5*E*). In our experiments, the minimum crack growth per cycle, dc/dn, that we measure is 0.4 nm $cycle^{-1}$. The linear regression of data estimates the fatigue threshold (Fig. 5 *E* and *F*). The fatigue threshold of PEA-$PMMA_{40}$ is 1,100 J m^{-2}, about seven times that of pure PEA (160 J m^{-2}). Under cyclic load, the crack does not bifurcate into long cracks, but the crack path is torturous (*SI Appendix*, Fig. S9).

The high fatigue threshold of the nanocomposite is understood as follows. In pure rubber, when a crack impinges on a polymer strand, the high tension is transmitted to the length of the strand. Once the strand breaks, the covalent energy of the entire strand is released (24).

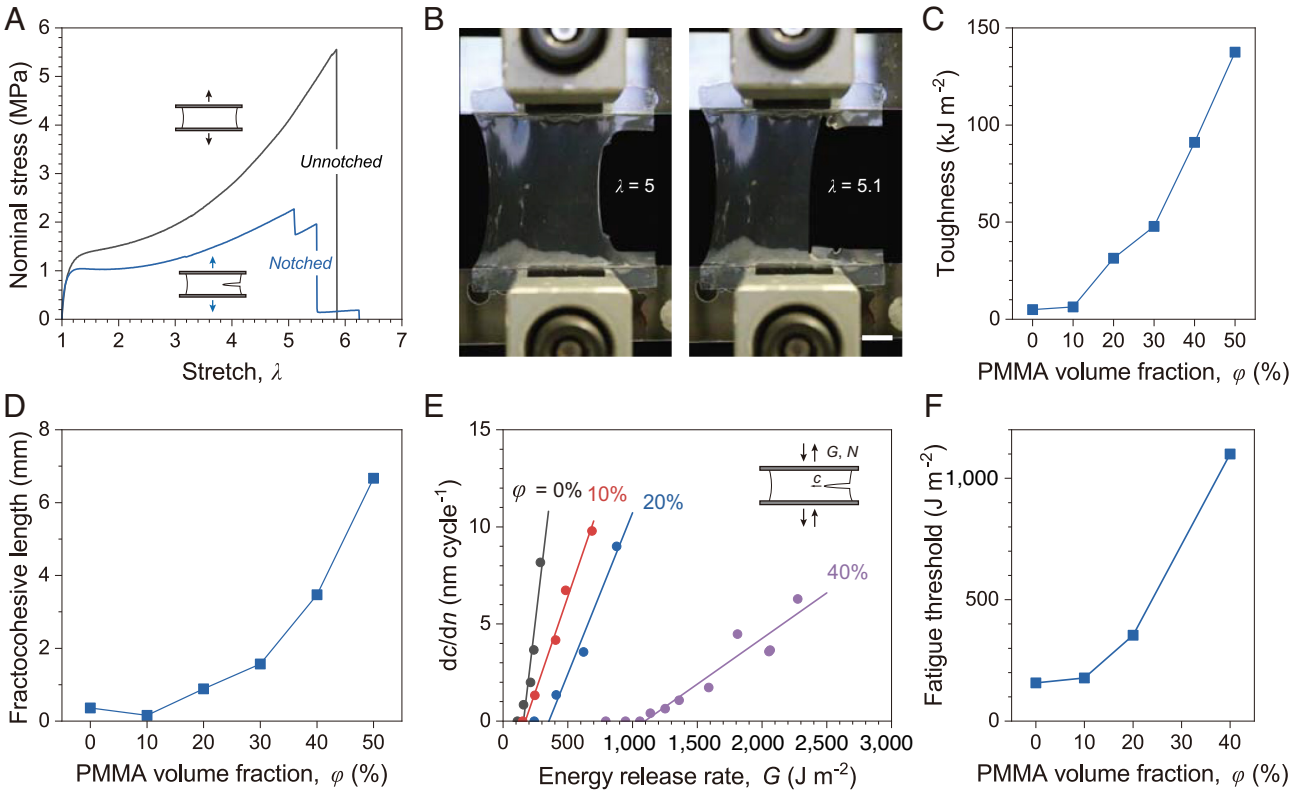

Fig. 5. Crack growth in rubber-glass nanocomposites under monotonic and cyclic loads. (*A*) The pure shear tests of the unnotched and notched samples of PEA-PMMA$_{40}$. (*B*) Photos of a precracked sample of PEA-PMMA$_{40}$ during the pure shear test under the monotonic load. The scale bar is 10 mm. (*C*) Toughness and (*D*) fractocohesive length as a function of PMMA volume fraction. (*E*) The fatigue crack extension per cycle, measured at various amplitudes of energy release rate. The load is cycled at 1 Hz. (*F*) Fatigue threshold as a function of PMMA volume fraction.

The fatigue threshold is estimated by the covalent energy stored in a layer of strand per unit area (10 ~ 100 J m^{-2}) (24). By contrast, in the nanocomposite, the rigid PMMA particles can further deconcentrate stress beyond a single layer of polymer strands (8). This multiscale stress deconcentration amplifies the fatigue threshold (8).

Notably, at ϕ = 10%, toughness, fractocohesive length, and fatigue threshold of the nanocomposite are similar to those of pure PEA. However, those three values increase substantially when ϕ = 20%. This observation is consistent with the theoretical prediction that particles percolate at 18% (16).

Although the method of mixed emulsion has been used before (14, 25–27), the coupling agent was absent in these previous works, so the cross-links and interlinks did not form. The present work shows that the coupling agent contributes to the mechanical properties and the stability of the nanostructures. In the absence of the silane coupling agent in PMMA, the fatigue threshold of the nanocomposite is lower than that of the nanocomposite with the silane coupling agent in PMMA (*SI Appendix*, Fig. S10). The absence of interlinks between PMMA particles and PEA chains leads to slippage during cyclic loading, compromising the ability of the percolated PMMA structure to transmit high tension from one particle to another. Furthermore, if the silane coupling agent is absent in PEA, the material will flow upon stretching (*SI Appendix*, Fig. S11).

The method of mixed emulsion can maintain the rubbery chains long in the final material by avoiding chain scission caused by high-intensity processes, such as extrusion and roll mill. The long polymer strands are entangled. The entanglements maintain modulus but do not impede stress deconcentration along the length of the polymer strand (20). Compared to pure PEA, a nanocomposite further amplifies modulus and fatigue threshold by percolated PMMA particles (Fig. 2*B*).

The rubber-glass nanocomposite made of mixed emulsion achieves significantly better mechanical performance than a composite made by solvent casting (*SI Appendix*, Fig. S12). The solvent-cast samples are also made of mixed emulsions but contain no silane coupling agent. A solvent-cast sample containing 40 vol.% of PMMA breaks at a stretch of 1.8 and exhibits a low tensile strength of 2.8 MPa. In the solvent-cast material, both PEA and PMMA particles dissolve in the solvent. After the solvent is removed, the material separates into two phases. The phases coarsen to a micron scale during solvent casting, and the sample is opaque.

The method of mixed emulsion is applicable to various manufacturing processes in open air, such as coat, cast, spray, print, and brush. During manufacturing, the silane coupling agent can interlink the nanocomposite to other materials.

By spin-coating the mixed emulsion and subsequently drying, a thin layer of the nanocomposite PEA-PMMA$_{40}$ with a thickness of ~5 μm is coated on a PDMS substrate (Fig. 6*A*). The PDMS substrate is pretreated by oxygen plasma to generate silanol groups on its surface. As water evaporates, the silane coupling agent interlinks the nanocomposite to the PDMS substrate. We use the T-peel test to measure the adhesion toughness between the coating and the substrate (Fig. 6*B*). The adhesion toughness is ~400 J m^{-2}, and the crack grows in the substrate, rather on the nanocomposite/substrate interface (Fig. 6*C*). Polymer coatings have broad applications, such as hydrophilic coatings for medical instruments and hermetic coatings for cardboard boxes and cups. Mixed emulsions may provide opportunities to engineer coatings with superior mechanical properties, as well as additional requirements, such as biocompatibility and biodegradability.

Nanocomposites with different compositions can be interlinked by the silane coupling agent. Two layers of nanocomposite with

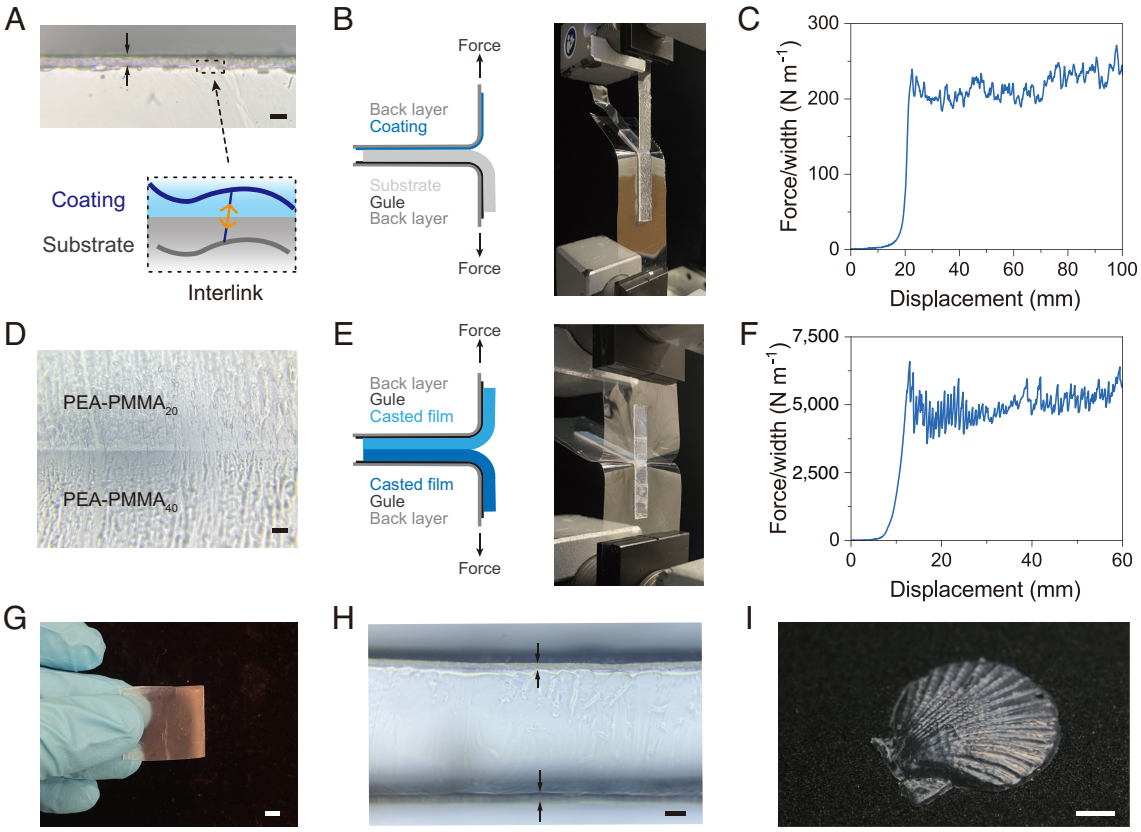

Fig. 6. The method of mixed emulsion is applicable to various open-air manufacturing processes. (*A*) Optical micrograph of a spin-coated layer of PEA-PMMA$_{40}$ on a PDMS substrate. The scale bar is 5 μm. (*B*) Sample geometry and photo of the T-peel test. (*C*) Force per unit width as a function of displacement of the T-peel test. (*D*) Sequentially casting layers of two nanocomposites, PEA-PMMA$_{20}$ and PEA-PMMA$_{40}$. The scale bar is 20 μm. (*E*) Sample geometry and photo of the T-degree peel test between the two nanocomposite layers. (*F*) Force per unit width as a function of displacement of the T-peel test. (*G*) Polyacrylamide hydrogel is dip-coated with PEA-PMMA$_{40}$. The scale bar is 10 mm. (*H*) Optical micrograph of the dip-coated nanocomposite on the hydrogel. The scale bar is 100 μm. (*I*) Cast the PEA-PMMA$_{40}$ using a mold of a complex shape. The scale bar is 5 mm.

different compositions can sequentially form by emulsion casting at 45 °C (Fig. 6*D*). Subsequent heating at 65 °C introduces interlinks between different layers. The T-degree peel test is conducted (Fig. 6*E*), showing an adhesion toughness ~10,000 J m^{-2} (Fig. 6*F*). It can be expected that with careful adjustment of the water content or addition of rheological modifier, the mixed emulsion can be a printable ink that offers customizable mechanical properties (28, 29). The excellent adhesion between different nanocomposites made of mixed emulsions opens a door for fabricating objects of prescribed spatial variations of compositions.

The mixed emulsion can also be used to dip-coat. We dip-coat a nanocomposite on a polyacrylamide hydrogel (Fig. 6 *G* and *H*). The polyacrylamide chains contain a silane coupling agent during its preparation (30). After dip-coating and subsequent drying, a layer of nanocomposite with ~ 30 μm thickness forms on the surface of the hydrogel (Fig. 6*H*). The hydrogel–elastomer hybrid can be made into an artificial axon where the elastomer coating retards the loss of water (31). Besides, taking advantage of the low viscosity of the emulsion, a complex shape with a fine feature can be made by emulsion casting (Fig. 6*G*).

The method of mixed emulsion can enable materials to gain other unconventional properties. Here, we present the potential of the method by fabricating a polymer nanocomposite with five separate glass transition temperatures (*SI Appendix*, Fig. S13). To achieve this, five separate emulsions, each containing a single species of polymer chains copolymerized with the silane coupling agent, are mixed and subsequently cast into a nanocomposite film. The film is prepared at 45 °C, at which four of the five emulsions are rubbery, so that enough chains are mobile to form a continuous film. Each glass transition temperature of the nanocomposite film corresponds to each species of polymer chains. Such a nanocomposite with the special thermal property holds potential applications in areas like multishape memory polymers (32) and soft machines (33). Additionally, mixed emulsions can be used to fabricate multifunctional nanocomposites, such as coatings that are highly conductive and stable in water (34).

The method of mixed emulsion can be compared with the other methods of manufacturing rubber-glass nanocomposites. A commonly used method uses block copolymers containing rubbery and glassy chain segments (35, 36). The morphology of the block copolymers is determined by thermodynamics (37). When the fraction of the glassy chains is low (<17%), the glassy chain segments self-assemble to be nanoparticles embedded in the rubbery matrix. However, with a higher fraction of the glassy chains, the glassy phases become cylindrical and even continuous or lamellae, and the material becomes a plastic. Consequently, the block copolymers cannot achieve high modulus, high stretchability, and high fatigue threshold simultaneously.

Conclusion

This paper reports rubber-glass nanocomposites fabricated using mixed emulsion. We fabricate the nanocomposites by mixing one emulsion of a rubbery polymer and another emulsion of a glassy polymer. In each emulsion, polymer chains are copolymerized with a small amount of silane coupling agent. As water evaporates, the silane coupling agent condensates, cross-linking rubbery chains and interlinking the rubbery chains to glassy particles. The

cross-links and interlinks stabilize the nanostructure and lead to superior properties of the nanocomposites. For example, the PEA-$PMMA_{40}$ nanocomposite simultaneously achieves high modulus (30 MPa), high toughness (91 kJ m^{-2}), and high fatigue threshold (1,100 J m^{-2}). The method of mixed emulsion divides the labor between the emulsion maker and the emulsion user. The maker can produce emulsions on a large scale in a facility that controls volatiles. The user can apply emulsions with neither volatiles nor high-intensity processes. Consequently, the method of mixed emulsion is compatible with various open-air manufacturing processes, such as coat, cast, spray, print, and brush. Additionally, the silane coupling agent can interlink the nanocomposites to other materials. The method can be used to fabricate objects of complex shapes, fine features, and prescribed spatial variations of compositions.

Materials and Methods

Preparation of Polymer Emulsions. Ethyl acrylate (EA, E9706) and methyl methacrylate (MMA, M55909) as monomers, ammonium persulfate (APS, 248614) as the thermal initiator, 3-(trimethoxysilyl)propyl methacrylate (TMSPMA, 440159) as the silane coupling agent, and sodium dodecyl sulfate (SDS, 436143) as the surfactant were purchased from Sigma-Aldrich and used without further purification. Distilled water was purchased from Poland Spring. The synthesis of PEA emulsion is presented as an example. 72 g EA and 17.1 μL TMSPMA (the TMSPMA-to-EA molar ratio is 10^{-4}) were mixed and ultrasonicated for 5 min to remove the dissolved oxygen. 0.415 g SDS (SDS-to-EA molar ratio is 2×10^{-3}), 0.016 g APS (APS-to-EA molar ratio is 10^{-4}), 168 g distilled water, and the mixture of EA and TMSPMA were added into a 500 mL round bottom flask (VWR, 10536) with a magnetic stirrer (51 mm in length, 58948-171). The whole mixture in the flask was stirred at 300 rpm and intensely purged with nitrogen for 10 min and then was sealed by a septum stopper. During this step, the mixture was already emulsified to be a white dispersion. Then, the flask was placed into a 65 °C oil bath and stirred at 300 rpm to start the radical polymerization. A syringe needle connected with a balloon was inserted into the septum stopper to balance the additional pressure by the exotherm during polymerization. After reacting for 8 h, the prepared emulsion was stored in a plastic jar made of high-density polyethylene (VWR, 16125-810) at room temperature. Preparation of PMMA emulsion is similar to that of PEA emulsion. The monomer is changed to MMA, and TMSPMA-to-MMA and APS-to-MMA molar ratios are changed to 10^{-3}. The emulsion is stable against cross-linking and coagulation for at least 8 mo. We did not see the sediments after the storage at room temperature for 8 mo, and the properties of the materials made of stored emulsions were identical to those made of fresh emulsions.

Dynamic Light Scattering. Dynamic light scattering was conducted on Malvern Zetasizer Pro. The test temperature is 25 °C. Emulsions are diluted by distilled water to be 1 mg mL^{-1} for the test.

Atomic Force Microscopy (AFM). AFM Imaging was conducted on a Cypher AFM (Asylum Research) in an AC mode and in the air. The AFM probe was 240AC-NA (Olympus Corporation). The sample was prepared by casting the emulsion on a clean silicon wafer with an area of 5 × 5 mm.

Preparation of the Nanocomposite Film. Eight grams of mixed emulsion was diluted with 8 g of distilled water and then poured into a polystyrene petri dish with a diameter of 100 mm (VWR, 25384-302). The petri dish was covered by two layers of filter papers with a diameter of 125 mm (VWR, 28320-100) and heated on a hot plate (45 °C) for 12 h. The nanocomposite film was peeled off from the petri dish and further heated at 65 °C in an oven for 24 h.

Tensile Test. The stress–stretch curve, elastic modulus, work of fracture, loading–unloading curve, and residual strain were measured by the uniaxial tensile test. The sample was cut into a dumbbell shape by a die cutter (Ace steel rule dies, ISO 527-2-5B). The total length of the sample is 35 mm, and the neck width is 2 mm. The sample was tested by Instron 5966 with a 10 kN load cell. The gauge length was 20 mm and was regarded as the sample's initial length. The stretch rate is 0.05 s^{-1}. The elastic modulus was obtained from the slope of the stress–stretch curve in the linear elastic region (stretch of <1.05). The work of fracture is calculated by integrating the stress–stretch curve.

Pure Shear Test. The toughness and fatigue threshold were measured by the pure shear test. The grippers were made of glass microscope slides (VWR, 16004-422). A sample of nanocomposite film was cut into a rectangular shape of area 60 mm × 40 mm. An adhesion promoter (Loctite 7701) was sprayed on both sides of the sample, and then, the sample was glued with the grippers using Krazy glue. The resulting sample has a free area of 60 mm × 10 mm. One sample was cut by a fresh razor blade (VWR, 55411-050) to form a 15 mm precrack, and the other one remains intact. While measuring toughness, the intact sample was stretched to obtain the strain energy density as a function of stretch, $W(\lambda)$, and the precracked sample was stretched to fracture to obtain the critical stretch, λ_c. The toughness was calculated by $W(\lambda_c)H_0$, where H_0 was the initial height of the sample. For the fatigue test, the strain energy density is measured from the stress–stretch curve of the unnotched sample after 1,000 cycles of loading and unloading. The notched sample was applied to a cyclic stretch of fixed amplitude. An amplitude of the stretch corresponds to an amplitude of energy release rate. Around 5,000 cycles were applied ahead of the measurement to form a consistent crack tip. The crack advance was measured by an optical microscope after additional 50,000 cycles and divided by the number of cycles to get the crack advance per cycle dc/dn. The resolution is 0.4 nm $cycle^{-1}$. The loading rate in the fatigue test is 1 Hz.

Preparation of the Nanocomposite Coating on the PDMS Substrate. The PDMS substrate of a diameter of 10 mm was made from the commercial precursor Sylgard 184, and the weight ratio of the base and curing agent was 15:1. The PDMS substrate was treated by oxygen plasma for 10 s using the Anatech Barrel Plasma System (Anatech LTD). The power of the oxygen plasma was 150 W, and the oxygen flow rate was 40 sccm. One gram of mixed emulsion was spin-coated on the pretreated PDMS substrate at 150 rpm, and the emulsion was dried by heating on a hot plate at 45 °C for 30 min and was then kept in an oven at 65 °C for 24 h.

T-Peel Test. PET films of 50 μm thickness were used as backing layers. For the peel test of the nanocomposite coating on the PDMS substrate, one PET film was pretreated by oxygen plasma and stuck on the freshly dried nanocomposite coating (45 °C). The sample was further heated at 65 °C for 24 h. Then another PET film was glued to PDMS using the adhesion promoter (Loctite 7701) and Krazy glue. The laminate was cut into a rectangular shape with a width of 10 mm. A crack was initiated along the coating using a razer blade. The two backing layers were pulled by a tensile tester (Instron 5966). For the peel test of the two nanocomposite layers, the PET backing layers were glued to the nanocomposite with the adhesion promoter (Loctite 7701) and Krazy glue. After the formation of the first layer, a scotch tape was stuck onto the surface of the first layer at one end. The scotch tape prevented the bonding in the corresponding area and served as a precrack. The adhesion toughness was calculated by double the plateau force divided by the sample width.

Data, Materials, and Software Availability. All study data are included in the article and/or supporting information.

ACKNOWLEDGMENTS. This work was supported by Harvard University MRSEC (DMR-2011754) and by the Air Force Office of Scientific Research (FA9550-20-1-0397). Z.C. acknowledges funding from the Academic Rising Star Program for PhD students in Zhejiang University.

Author affiliations: [a]John A. Paulson School of Engineering and Applied Sciences, Harvard University, Cambridge, MA 02138; and [b]State Key Laboratory of Chemical Engineering, College of Chemical and Biological Engineering, Zhejiang University, Hangzhou 310058, China

1. G. R. Hamed, Reinforcement of rubber. *Rubber Chem. Technol.* **73**, 524–533 (2000).
2. W.-C. Lin, W. Fan, A. Marcellan, D. Hourdet, C. Creton, Large strain and fracture properties of poly(dimethylacrylamide)/silica hybrid hydrogels. *Macromolecules* **43**, 2554–2563 (2010).
3. A. C. Balazs, T. Emrick, T. P. Russell, Nanoparticle polymer composites: Where two small worlds meet. *Science* **314**, 1107–1110 (2006).
4. D. De, A. N. Gent, Tear strength of carbon-black-filled compounds. *Rubber Chem. Technol.* **69**, 834–850 (1996).

5. A. N. Gent, *Engineering with Rubber: How to Design Rubber Components* (Carl Hanser Verlag GmbH Co KG, 2012).
6. X. Bao *et al.*, Low-intensity mixing process of high molecular weight polymer chains leads to elastomers of long network strands and high fatigue threshold. *Soft Matter* **19**, 5956–5966 (2023).
7. H. Fries, R. R. Pandit, Mastication of rubber. *Rubber Chem. Technol.* **55**, 309–327 (1982).
8. J. Steck, J. Kim, Y. Kutsovsky, Z. Suo, Multiscale stress deconcentration amplifies fatigue resistance of rubber. *Nature* **624**, 303–308 (2023).
9. C. Li, H. Yang, Z. Suo, J. Tang, Fatigue-resistant elastomers. *J. Mech. Phys. Solids* **134**, 103751 (2020).
10. N. A. Fleck, K. J. Kang, M. F. Ashby, Overview no. 112: The cyclic properties of engineering materials. *Acta Metall. Mater.* **42**, 365–381 (1994).
11. Z. Wang *et al.*, Stretchable materials of high toughness and low hysteresis. *Proc. Natl. Acad. Sci. U.S.A.* **116**, 5967–5972 (2019).
12. P. A. Steward, J. Hearn, M. C. Wilkinson, An overview of polymer latex film formation and properties. *Adv. Colloid Interface Sci.* **86**, 195–267 (2000).
13. A. J. Silvaroli *et al.*, Tough, transparent, photocurable hybrid elastomers. *ACS Appl. Mater. Interfaces* **12**, 44125–44136 (2020).
14. J. Feng, M. A. Winnik, R. R. Shivers, B. Clubb, Polymer blend latex films: Morphology and transparency. *Macromolecules* **28**, 7671–7682 (1995).
15. S. Torquato, T. M. Truskett, P. G. Debenedetti, Is random close packing of spheres well defined? *Phys. Rev. Lett.* **84**, 2064–2067 (2000).
16. M. J. Powell, Site percolation in random networks. *Phys. Rev. B* **21**, 3725–3728 (1980).
17. E. Guth, Theory of filler reinforcement. *Rubber Chem. Technol.* **18**, 596–604 (1945).
18. A. P. Kotula, K. B. Migler, Evaluating models for polycaprolactone crystallization via simultaneous rheology and Raman spectroscopy. *J. Rheol.* **62**, 343–356 (2018).
19. A. J. Silvaroli *et al.*, Role of nanoscale heterogeneity in the mechanical performance of hybrid elastomers. *Macromolecules* **56**, 4075–4086 (2023).
20. J. Kim, G. Zhang, M. Shi, Z. Suo, Fracture, fatigue, and friction of polymers in which entanglements greatly outnumber cross-links. *Science* **374**, 212–216 (2021).
21. R. Bai, J. Yang, X. P. Morelle, Z. Suo, Flaw-insensitive hydrogels under static and cyclic loads. *Macromol. Rapid Commun.* **40**, 1800883 (2019).
22. C. Chen, Z. Wang, Z. Suo, Flaw sensitivity of highly stretchable materials. *Extreme Mech. Lett.* **10**, 50–57 (2017).
23. J. Liu *et al.*, Polyacrylamide hydrogels. II. Elastic dissipater. *J. Mech. Phys. Solids* **133**, 103737 (2019).
24. G. J. Lake, A. G. Thomas, D. Tabor, The strength of highly elastic materials. *Proc. R. Soc. London Ser. A* **300**, 108–119 (1997).
25. L. M. Robeson, R. M. Berner, Mechanical properties of emulsion polymer blends. *J. Polym. Sci. Part B: Polym. Phys.* **39**, 1093–1106 (2001).
26. M. A. Winnik, Latex film formation. *Curr. Opin. Colloid Interface Sci.* **2**, 192–199 (1997).
27. C. Tongyu *et al.*, Study of particle morphology in polymer emulsions and their minimum film formation temperatures. *J. Appl. Polym. Sci.* **41**, 1965–1972 (1990).
28. B. M. Rauzan, A. Z. Nelson, S. E. Lehman, R. H. Ewoldt, R. G. Nuzzo, Particle-free emulsions for 3D printing elastomers. *Adv. Funct. Mater.* **28**, 1707032 (2018).
29. M. Lukić, J. Clarke, C. Tuck, W. Whittow, G. Wells, Printability of elastomer latex for additive manufacturing or 3D printing. *J. Appl. Polym. Sci.* **133**, 42931 (2016).
30. Q. Liu, G. Nian, C. Yang, S. Qu, Z. Suo, Bonding dissimilar polymer networks in various manufacturing processes. *Nat. Commun.* **9**, 846 (2018).
31. P. Le Floch *et al.*, Wearable and washable conductors for active textiles. *ACS Appl. Mater. Interfaces* **9**, 25542–25552 (2017).
32. Y. Luo, Y. Guo, X. Gao, B.-G. Li, T. Xie, A general approach towards thermoplastic multishape–memory polymers via sequence structure design. *Adv. Mater.* **25**, 743–748 (2013).
33. S. Zhuo *et al.*, Complex multiphase organohydrogels with programmable mechanics toward adaptive soft-matter machines. *Sci. Adv.* **6**, eaax1464 (2020).
34. G. Zhang, Z. Chen, C. H. Ahn, Z. Suo, Conducting polymer coatings prepared by mixed emulsions are highly conductive and stable in water. *Adv. Mater.*, 2306960 (2024).
35. F. S. Bates *et al.*, Multiblock polymers: Panacea or Pandora's Box?. *Science* **336**, 434–440 (2012).
36. J. Fang, S. Wang, Y. Luo, One-pot synthesis of octablock copolymers of high-molecular weight via RAFT emulsion polymerization. *AIChE J.* **66**, e16781 (2020).
37. F. S. Bates, G. H. Fredrickson, Block copolymer thermodynamics: Theory and experiment. *Annu. Rev. Phys. Chem.* **41**, 525–557 (1990).